Solution Structure of the Reps1 EH Domain and Characterization of Its Binding to NPF Target Sequences[†,‡]

Soyoun Kim, Donald N. Cullis, Larry A. Feig, and James D. Baleja*

Department of Biochemistry, Tufts University School of Medicine, 136 Harrison Avenue, Boston, Massachusetts 02111

Received November 27, 2000; Revised Manuscript Received April 12, 2001

ABSTRACT: The recently described EH domain recognizes proteins containing Asn-Pro-Phe (NPF) sequences. Using nuclear magnetic resonance (NMR) data, we determined the solution structure of the EH domain from the Reps1 protein and characterized its binding to linear and cyclic peptides derived from a novel targeting protein. The structure calculation included 1143 distance restraints and 122 angle restraints and resulted in structures with a root-mean-square deviation of 0.40 ± 0.05 Å for backbone atoms of superimposed secondary structural elements. The structure comprises two helix−loop−helix motifs characteristic of EF-hand domains. Titration data with NPF-containing peptides showed evidence of intermediate exchange on the NMR chemical shift time scale, which required an analysis that includes curve fitting to obtain accurate equilibrium constants and dissociation rate constants. The cyclic and linear peptides bound with similar affinities (K_d = 65 ± 17 and 46 ± 14 μM, respectively) and to the same hydrophobic pocket formed between helices B and C. The cyclic peptide formed a complex that dissociated more slowly (k_{off} = 440 ± 110 s^{-1}) than the linear peptide (k_{off} = 1800 ± 250 s^{-1}), but had little change in affinity because of the slower rate of association of the cyclic peptide. In addition, we characterized binding to a peptide containing a DPF sequence (K_d = 0.5 ± 0.2 mM). The characterization of binding between the Reps1 EH domain and its target proteins provides information about their role in endocytosis.

Protein recognition modules often mediate the assembly of macromolecular complexes. The Eps15 homology (EH)[1] domain was first recognized as a segment repeated three times within the sequence of the Eps15 protein, a substrate for phosphorylation by the EGF receptor (*1*). Subsequently, the EH domain has been identified in a large and growing number of proteins ranging in organisms from yeast to humans. The majority of the EH domain-containing proteins are involved in endocytosis or vesicle transport (*2*). The EH domain comprises approximately 100 amino acid residues and contains two EF-hand motifs (*3*) and a C-terminal proline-rich region (*1*). Most EH domains mediate their functions through binding other proteins that contain the tri-amino acid residue Asn-Pro-Phe (NPF) sequence. Although many target proteins contain multiple NPF sequences, EH domains have also been implicated in binding the Asp-Pro-Phe (DPF) sequence (*4, 5*).

Reps1, a protein containing a single EH domain, was recently identified by yeast two-hybrid experiments as a binding partner of RalBP1, a downstream target protein of the Ral GTPase. RalBP1 is also a GTPase-activating protein for CDC42 and Rac GTPases (*6*). GTP-Ral proteins also bind to RalBP1. The Ral proteins can be activated by Ras (*7*) and are also implicated in endocytosis even though they do not contain EH domains (*4*). The Reps1 protein is tyrosine phosphorylated in response to EGF receptor stimulation (*6*). In addition, Reps1 has the capacity to form complexes with the SH3 domains of adapter proteins Crk and Grb2, which may link Reps1 to an EGF-responsive tyrosine kinase. Reps1 may thus coordinate the cellular actions of activated EGF receptors and Ral-GTPases.

The exact role of Reps1 in endocytosis is not known, although more is understood about a closely related but distinct protein, POB1. POB1 contains similar protein domains arranged in a similar order (*8*), but it is different in that the full-length protein is nearly 200 amino acids shorter. The amino acid sequences of the EH domains are 74% identical. The EH domain of POB1 binds directly to Epsin, a protein bearing several NPF sequences (*9*). RalBP1, POB1, Epsin, and Eps15 form a complex with α-adaptin of AP-2 in Chinese hamster ovary cells that is dissociated by phosphorylation of the first four components (*9*). In particular, phosphorylation of Epsin arrests receptor-mediated endocytosis during mitosis by disassembly of its complex with POB1 and α-adaptin. It is not yet clear how Reps1 and POB1 differ biochemically; however, their distinct EH domains present the potential for multiple signals emanating from RalBP1.

The three-dimensional structure has been determined for the EH domain from POB1 (*10*). The backbone atoms of superimposed secondary elements have an rms deviation of 0.76 ± 0.49 Å, but little information is known about the

[†] Supported by Research Project Grant 00-087-01-GMC from the American Cancer Society (J.D.B.) and Grant R01 GM47717 from the National Institutes of Health (L.A.F.).

[‡] Atomic coordinates have been deposited with the Research Collaboratory for Structural Bioinformatics Protein Data Bank (entry 1FI6).

* To whom correspondence should be addressed. Phone: (617) 636-6872. Fax: (617) 636-2409. E-mail: jim.baleja@tufts.edu.

[1] Abbreviations: EH, Eps15 homology; GST, glutathione *S*-transferase; HSQC, heteronuclear single-quantum coherence; NMR, nuclear magnetic resonance; NOE, nuclear Overhauser effect; NOESY, NOE spectroscopy; rms, root-mean-square.

10.1021/bi002700m CCC: $20.00
Published on Web 05/15/2001

conformation of its C-terminal proline-rich region. Higher-resolution structures have been obtained for the first EH (EH_1) domain of murine Eps15 (*11*) and for the second and third EH (EH_2 and EH_3) domains of human Eps15 with rms deviations of superimposed secondary elements of 0.59, 0.26, and 0.33 Å, respectively (*12*, *13*). These structures each comprise two helix−loop−helix motifs characteristic of calcium-binding EF-hand domains. Sequence analysis indicates that not all the EF-hands are capable of binding calcium because of mutations of the calcium-liganding residues in the loop. The Eps15 EH_1 domain, for example, binds no calcium with appreciable affinity (*11*), whereas the second Eps15 EH_2 domain has been shown to bind a single calcium using the second EF-hand (*12*). The second EF-hand calcium binding motifs of the POB1 and Reps1 EH domains each have the conserved residues needed for calcium binding in the second EF-hand, but the first EF-hand does not, indicating that only one calcium ion can be bound. The sequences of the Eps15 EH domains are 26−38% identical with that of either the POB1 or Reps1 EH domain. All these EH domains have been shown to interact with NPF-containing peptides.

NMR spectroscopy is a powerful tool for understanding many different aspects of protein−ligand interactions, ranging from structural information about the protein−ligand complex to dynamic, kinetic, and thermodynamic aspects of ligand binding. The method provides an approach to identifying the amino acid residues that constitute the protein interaction site by monitoring differential line broadening (*14*) and chemical shift changes in $^{15}N-^{1}H$ HSQC spectra (*15*) upon ligand binding.

The effect of binding on the appearance of the NMR resonances is determined by the relationship between the exchange rate constant, k, for the interconversion of the bound and free states and the corresponding difference in resonance frequencies, $\Delta\delta$. At substoichiometric ratios of peptide to protein under conditions of slow exchange where $k \ll \Delta\delta$, distinct signals are observed for each of the two states of the protein. If the exchange between the bound and free states is fast (i.e., $k \gg \Delta\delta$), a single resonance is observed at the population-weighted average chemical shift of the nuclei in two states. When the exchange between the bound and free ligand states (or between different bound forms of the ligand) is in the intermediate exchange regime ($k \approx \Delta\delta$), there is substantial line broadening. Typically, the observable changes of frequencies upon binding are on the order of 0.02−1 ppm (i.e., 10−500 Hz for ^{1}H resonances at a field strength of 500 MHz). The presence of broadening thus indicates that there are dynamic processes occurring with lifetimes of roughly 2−100 ms. Under conditions of intermediate exchange, the peak position may no longer accurately reflect the weighted average between free and bound forms of the protein (*16*). A full analysis of the effects of intermediate exchange often results in determination of not only the equilibrium dissociation constant but also the rate of association. The rate of association of the EH domain with its target peptide may be controlled by random collisions governed by the rate of diffusion. On the other hand, a slower rate of complex assembly signifies that conformational changes are required by the protein to bind its NPF target peptide or by the peptide to bind to the protein (*17*).

To characterize the properties of the Reps1 EH domain, we determined its structure by multidimensional heteronuclear NMR spectroscopy. Methods are presented for analyzing titration data in the presence of intermediate exchange on the NMR chemical shift time scale. The site of interaction on the EH domain for NPF-bearing amino acid sequences was determined, as well as the on and off rates and equilibrium affinity constants for complex formation.

MATERIALS AND METHODS

Peptide Synthesis. A peptide containing the target NPF sequence of the EH domain, Ac-YEST**NPF**TAKF-NH_2 (**NPF**$_{lin}$), was synthesized as well as two homologous peptides, YEST**DPF**TAKF and YEST**NPY**TAKF, that contain site-specific mutations relative to the parent **NPF**$_{lin}$ peptide. We also synthesized a cyclic version of **NPF**$_{lin}$ on the basis of observations that EH domains from the homologous protein, Intersectin, more tightly bind a cyclic peptide than its linear counterpart (*18*) and that the Reps1 EH domain was observed to bind both linear and cyclic NPF-containing peptides (Y. Yamabhai and B. Kay, personal communication). The cyclic peptide, EYECT**NPF**TAKC (**NPF**$_{cyc}$), was designed by substituting Ser^{3} and Phe^{11} of the linear peptide by cysteines for disulfide bond formation. Since the oxidized, disulfide cross-linked peptide was predicted to be insoluble, an additional charged Glu residue from the Reps1 target protein sequence was included on the N-terminus. All peptides were purified by C_{18} reversed-phase high-performance liquid chromatography (HPLC), and identities were confirmed using matrix-assisted laser desorption ionization (MALDI) mass spectrometry.

Sample Preparation. Perdeuterated dithiothreitol (DTT_{d10}), D_2O (99%), and imidazole (imidazole$_{d4}$) were obtained from Cambridge Isotope Laboratories (Andover, MA). The EH domain (residues 227−318) from the Reps1 protein (*19*) was expressed with a five-amino acid N-terminal extension derived from the cloning vector and purified as described previously (*20*). The sequence is renumbered as residues 1−97. A human DNA sequence (GenBank accession number A121384) predicts an EH domain of identical sequence. Samples included 1.0−1.5 mM protein, 10 mM NaCl, 2 mM $CaCl_2$, 0.01% NaN_3, 10 mM imidazole$_{d4}$ at pH 6.7 ± 0.1, and 5 mM DTT_{d10} (except for ones containing the cyclic peptide). Samples were stable for at least 10 days at 30 °C and several months at 4 °C. Stock peptide solutions were 10 mM in the same buffer. Concentrations were determined by UV spectroscopy (*21*).

Structure Determination. NMR resonance assignments were obtained using homonuclear and heteronuclear multidimensional spectra collected on Bruker AMX-500 and Avance-600 NMR spectrometers (*20*). Stereospecific assignments for the methyl groups of Val and Leu residues were obtained through analysis of a two-dimensional constant time (CT) $^{1}H-^{13}C$ HSQC spectrum acquired on a 10% ^{13}C-labeled sample. Geminal β protons (43 of 73) were also stereospecifically assigned (*20*).

NOE cross-peak intensities were determined from homonuclear two-dimensional and heteronuclear three-dimensional (^{15}N-separated and ^{13}C-separated) NOESY spectra collected using mixing times of 80 and 150 ms. NOE cross-peak intensities were designated strong, medium, or weak, and given upper bounds of 3.0, 4.0, and 5.0 Å and lower bounds of 1.7, 2.7, and 3.7 Å, respectively. Pseudoatom corrections

were added to the upper bounds for degenerate methyl, methylene, and aromatic ring protons. When necessary, 0.5 Å was added to correct for spin diffusion or for overlapping resonances (*22*).

Backbone dihedral angle (ϕ) restraints were measured from the splitting of amide cross-peaks in a $^1H-^{15}N$ HSQC spectrum that was resolution enhanced by multiplication with a squared sine bell window function shifted by 30° and applied over 4K points in the proton dimension. The backbone torsion angle ϕ was restrained to $-58 \pm 15°$ for $^3J_{HN\alpha}$ values of <5.5 Hz and to $-120 \pm 20°$ for $^3J_{HN\alpha}$ values of >9.5 Hz. χ_1 angles were obtained from a three-dimensional HNHB experiment and, where applicable, from a comparison of the H$\alpha-$Hβ coupling constants ($^3J_{\alpha\beta}$) and the H$\alpha-$Hβ and H$\beta-$HN NOE intensities.

The initial structure calculation included 1143 distance restraints (362 intraresidue, 353 sequential, 164 medium-range, and 264 long-range), 70 ϕ angle restraints, and 52 χ_1 angle restraints. Eighty structures were calculated using r^{-6} summation in a restrained molecular dynamics simulated annealing protocol within the X-PLOR 3.84 software package (*23*) using the PROLSQ force field (*24*). The final calculation included six distance restraints between the calcium and coordinating oxygen atoms based on average distances in the high-resolution crystal structures of EF-hand proteins (*25*, *26*). Their inclusion did not significantly perturb the structure of the protein backbone or violate the many NOE cross-peaks involving residues in the loop region. Forty structures were identified with NOE violations of <0.2 Å and dihedral violations of <5 Å, and the 30 with the lowest overall NOE violations were further analyzed. Coordinates have been deposited in the Protein Data Bank as entry 1FI6.

NPF Peptide Titration. The uniformly ^{15}N-labeled EH domain (0.6 mM) was titrated with peptides from 10 mM stocks. $^1H-^{15}N$ HSQC spectra were collected at peptide:protein molar ratios of 0, 0.25, 0.5, 0.75, 0.85, 0.95, 1.0, 1.1, 1.25, 1.5, and 2.0.

Titration Analysis in Fast Exchange. One to one binding of protein, P, and peptide, L, to form a protein−peptide complex, PL, can be expressed as

$$[P] + [L] \leftrightharpoons [PL] \quad (1)$$

The equilibrium dissociation constant, K_d, for this reaction is

$$K_d = k_{off}/k_{on} = ([P][L])/[PL] \quad (2)$$

Where $P_o = [P] + [PL]$ and $L_o = [L] + [PL]$, K_d and [PL] can be calculated from

$$K_d = (P_o - [PL])(L_o - [PL])/[PL] \quad (3)$$

$$[PL] = {}^1/_2\{L_o + P_o + K_d - [(L_o + P_o + K_d)^2 - 4L_oP_o]^{1/2}\} \quad (4)$$

If the product of the lifetime of the bound species, τ_b, and the difference in chemical shift between free and bound ($\delta_b - \delta_f$) is much less than 1, then $\delta_{obs} = \delta_f f_f + \delta_b f_b$, where δ_f is the chemical shift of the unbound species, δ_b is that of the bound species, and f_f and f_b are the fractions bound and unbound, respectively ($f_f + f_b = 1$). The observed change in chemical shift during the titration of the free EH domain with peptide is given by

$$\Delta\delta = \frac{[PL]}{P_o}(\delta_b - \delta_f) \quad (5)$$

After substitution of eq 4 into eq 5, the titration data were fitted by adjusting K_d and $\delta_b - \delta_f$ using a Microsoft Excel spreadsheet program and by monitoring the sum of the squared differences (χ^2) between the calculated chemical shift and the observed. The titration data were fitted independently using CRVFIT (a nonlinear least-squares fitting program obtained from R. Boyko and B. D. Sykes).

A dissociation rate constant (k_{off}) can be estimated from the line broadening due to chemical exchange. The observed line width in radians per second at half-height of the resonance, $\Delta\upsilon_{obs}$, is given by

$$\Delta\upsilon_{obs} = f_f(\Delta\upsilon_f) + f_b(\Delta\upsilon_b) + f_f^2 f_b^2(\Delta\delta)^2(\tau_f + \tau_b) \quad (6)$$

where $\Delta\upsilon_f$ and $\Delta\upsilon_b$ are the line widths at half-height of the free and bound protein, respectively, $\Delta\delta$ is the chemical shift difference between bound and unbound forms, and τ_f and τ_b are the lifetimes of the free and bound forms, respectively (*27*). Since the populations are related to the lifetimes by

$$f_f = \tau_f/(\tau_f + \tau_b) \text{ and } f_b = \tau_b/(\tau_f + \tau_b) \quad (7)$$

Equation 6 can be written as

$$\Delta\upsilon_{obs} = f_f(\Delta\upsilon_f) + f_b(\Delta\upsilon_b) + f_f^2 f_b(\Delta\delta)^2 1/k_{off} \quad (8)$$

where k_{off} is the dissociation rate constant ($=1/\tau_b$). The data were fitted by adjusting $\Delta\upsilon_f$, $\Delta\upsilon_b$, k_{off}, and $\delta_b - \delta_f$ using a Microsoft Excel spreadsheet program and by monitoring the sum of the squared differences (χ^2) between the calculated line width and the observed.

Titration Analysis with Consideration of All Exchange Regimes. In the intermediate exchange region, the line shape is complicated and there is no simple expression such as eq 5 to calculate the observed position of the chemical shift (*16*). However, calculating line shapes explicitly allows the simulation of the signal amplitude as a function of frequency for a particular ligand concentration for all exchange regimes (*16*, *28*). The function outlined by Nakagawa (*16*, *28*) simulates each line shape based on the parameters $\delta_b - \delta_f$, the line width at half-height, k_{off}, and f_b, and gives the relative intensity with respect to the signal position between the free and bound states. The fraction bound, f_b, can be calculated from the K_d with eqs 3 and 4. To simulate a binding curve, the frequency of maximal signal amplitude was determined for each titration point using a Microsoft Excel spreadsheet (*29*). Although line widths were experimentally determined and varied from 25 to 50 Hz, the resultant maximum peak position was insensitive to this parameter. The experimental binding data were fitted by adjusting $\delta_b - \delta_f$, k_{off}, and K_d and by monitoring the sum of the squared differences (χ^2) between the calculated chemical shift and the observed.

RESULTS

Structure Description. The solution structure of the Reps1 EH domain was determined using high-resolution multidimensional heteronuclear NMR spectroscopy following es-

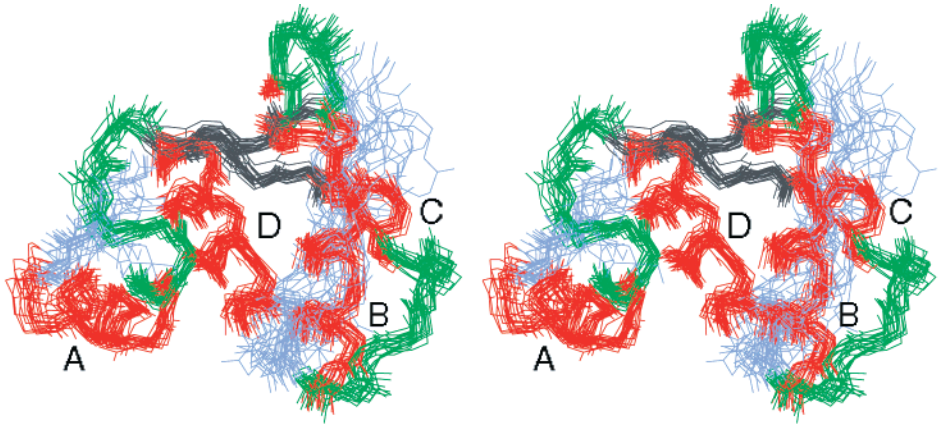

FIGURE 1: Stereo representation of 20 superimposed Reps1 EH domain structures. The four helices of the domain, shown in red, are labeled A−D. Residues that constitute the β-sheet are shown in black, whereas connecting elements are in green and less well-ordered residues in blue. The rms deviation from the mean for backbone atoms of superimposed secondary structural elements was 0.40 ± 0.05 Å.

Table 1: Structure Statistics for the Reps1 EH Domain[a]

Structure Generation			
distance restraints		dihedral angle restraints	
intraresidue NOEs[b]	362	ϕ	70
interresidue NOEs	353	χ_1	52
medium-range NOEs	164		
long-range NOEs	264		
calcium ligation	6		
Ramachandran Analysis[c]			
most favorable region	78.8	generously allowed region	1.2
additionally allowed region	20.0	disallowed region	0.0
Average Energies (kcal/mol)			
E_{total}	−850 ± 50	$E_{dihedral}$	3 ± 0.5
E_{NOE}	20 ± 5		
Restraint Violations			
largest NOE violation/ structure < 0.2 Å		largest angle violation/ structure < 5°	
rmsd from Idealized Geometry			
bonds (Å)	0.003 ± 0.0001	angles (deg)	0.45 ± 0.01
improper angles (deg)	0.36 ± 0.02		

Atomic rmsd (Å)[d]		
	backbone	all heavy atoms
secondary structure elements[e]	0.40 ± 0.05	0.9 ± 0.1

[a] All statistics are reported as averages for the 30 structures with the lowest NOE violation energies. [b] Medium-range NOEs are between residues separated by two to four residues, and long-range NOEs are between residues separated by five or more residues. [c] Prolines and glycines are not included. [d] The average root-mean-square deviations for the final 30 structures from the average structure. [e] Residues 12−22, 29−41, 50−57, and 64−80.

tablished protocols (*30*). The large number of distance restraints (1143) and dihedral restraints (122) yielded well-defined solution structures with a root-mean-square (rms) deviation in secondary structure elements of 0.40 ± 0.05 Å for the backbone atoms and 0.9 ± 0.1 Å for all heavy atoms (Table 1). A total of 78.8% of the residues were in the most favored region of the Ramachandran plot, 20% in the additionally allowed region, 1.2% in the generously allowed region, and 0% in the disallowed region (*31*). Superimposition of the ensemble of structures on the structure with the lowest NOE violation energy reveals two helix−loop−helix motifs (Figure 1). Helices αA−αD span residues Asp[10]−Phe[20], Gly[33]−Thr[41], Leu[50]−Ser[57], and Asp[68]−Arg[80], respectively. Two short strands of three residues each (Gly[29]−Ile[31] and Ala[64]−Thr[66]) form a small antiparallel β-sheet. The two loops of the EF-hand substructures associate through main chain hydrogen bonds and side chain interactions between residues Ile[31] and Leu[65] in the β-sheet region (Figure 2). The first helix (αA) lies roughly perpendicular to the other three helices (with angles of 117.9 ± 3.6°, −106.8 ± 4.2°, and 114.3 ± 3.7°, respectively) and contacts primarily the centrally located fourth helix (αD). The second (αB) and fourth helices are nearly parallel (−28 ± 3.2°), whereas the third helix (αC) is slightly tilted relative to helices B and D (128 ± 2.9° and 138.5 ± 3.3°, respectively). The structure of the proline-rich C-terminal region is interesting because this region is known to be required for NPF peptide binding (*27*). Although the resolution of this region is lower than for the helical portion of the domain (Figure 1), the proline-rich element clearly zigzags over the αC and αD helices, thus juxtaposing the N- and C-termini (Figure 2).

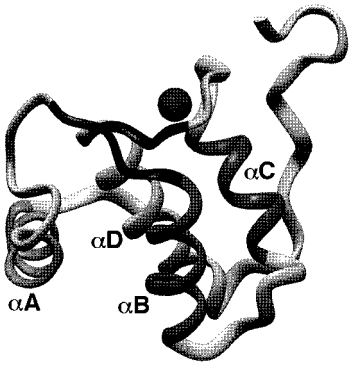

FIGURE 2: Ribbon diagram of the Reps1 EH domain structure. Secondary structural elements include four α-helices, in gray (αA, Asp[10]−Phe[20]; αB, Gly[33]−Thr[41]; αC, Leu[50]−Ser[57]; and αD, Asp[68]−Arg[80]), and a short antiparallel β-sheet, in black (Gly[29]−Ile[31] and Ala[64]−Thr[66]). The bound calcium ion is shown as a space-filling representation. The image was created using INSIGHT II (Molecular Simulations, Inc.).

The primary sequence data imply that the Reps1 EH domain has one calcium-binding site in the second helix−loop−helix motif (Asp[58], Asp[60], Asp[62], Ala[64], Thr[66], and Glu[69]). The presence of a bound calcium ion was evidenced by the unusual chemical shift of the Gly[63] amide proton at 10.66 ppm. The downfield chemical shift of the amide proton of glycine, which is in the middle of the calcium-binding motif, is a well-known signature for calcium binding in EF-

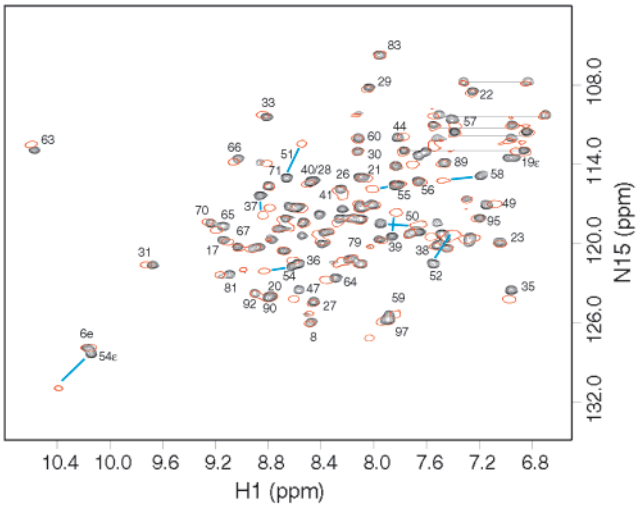

FIGURE 3: Superimposed $^{15}N-^{1}H$ HSQC spectra of the Reps1 EH domain with 0 (black) and 1 equiv (red) of the **NPF**$_{cyc}$ peptide (Ac-EYECTNPFTAKC-NH_2). The 500 MHz spectra were collected at 30 °C on samples containing approximately 0.6 mM EH domain.

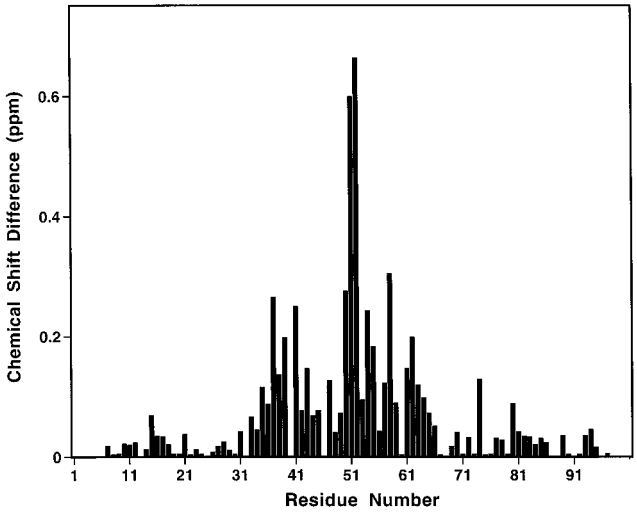

FIGURE 4: Histogram depicting the change in ^{15}N and ^{1}H chemical shifts of the backbone amide resonances of the Reps1 EH domain upon addition of 1 equiv of **NPF**$_{cyc}$. The chemical shift difference (parts per million) was calculated from the absolute value of the change in the ^{1}H chemical shift plus 0.2 times the absolute value of the change in the ^{15}N chemical shift.

hands (*32*). The structures were consistent with a single calcium ion bound to the expected region using a standard calcium ion binding geometry (see Materials and Methods) (*33*).

Identification of the NPF-Binding Pocket. Using the yeast two-hybrid system, a new Reps1 target protein has been identified that contains three NPF sequences (D. N. Cullis and L. A. Feig, unpublished experiments). A survey of the target proteins of EH domains reveals that only the core NPF is conserved (*27*). Few preferences are noted for amino acids adjacent to NPF except that negatively charged residues are never found, and that a serine or threonine residue sometimes precedes NPF. Since the first and third NPF sequences of the Reps1 target protein contain adjacent negatively charged residues, but the second NPF motif does not, and because the second NPF motif has the semiconserved S or T residue preceding the NPF sequence, but the first and third NPF sequences do not, we synthesized the peptide YESTNPFTAKF (**NPF**$_{lin}$) corresponding to the second NPF motif (*27*). To understand the molecular specificity of the Reps1 EH domain, we also synthesized two 11-residue peptides (**DPF** and **NPY**) with single-amino acid replacements relative to **NPF**$_{lin}$ as described in Materials and Methods.

Yamabhai et al. (*18*) observe that for the Intersectin EH domain cyclic NPF-containing peptides show a higher affinity than their linear counterparts, possibly by stabilizing a turn conformation commonly observed in asparagine-proline dipeptides within proteins. In addition, the K_d for the second EH domain of Eps15 for the linear sequence (PTGSSSTNPFL) from the RAB protein (**NPF**$_{RAB}$) is 560 $\pm$ 40 μM (*12*), whereas a cyclic version (SSDCTNPFRSCWRS) shows a much greater affinity ($K_d = 12 \pm 2$ μM) (*34*). Because of these observations, we also synthesized a cyclic peptide, **NPF**$_{cyc}$, in which Ser^3 and Phe^{11} of the linear peptide were replaced with cysteines, which readily formed a disulfide bond.

We titrated **NPF**$_{cyc}$ into the ^{15}N-labeled EH domain and monitored progressive changes of ^{1}H and ^{15}N resonances with a series of ^{15}N HSQC spectra (Figure 3). The observed chemical shift differences are shown for each residue in Figure 4. A separate titration with **NPF**$_{lin}$ showed the same pattern of chemical shift changes as that observed for **NPF**$_{cyc}$, indicating the peptides interact with the same residues of the EH domain. At saturation, the resonances of the complex with **NPF**$_{cyc}$ generally shifted more (~60%) and were better resolved than the complex with **NPF**$_{lin}$. Lys^{37}, Phe^{39}, Leu^{50}, Ser^{51}, His^{52}, Trp^{54}, Glu^{55}, and Asp^{58} had the largest changes and, in accordance with eq 8, showed exchange broadening during titration and became sharper when approaching the 1:1 peptide:protein ratio (i.e., $f_b \sim 1$). Phe^{40} was also likely to have large chemical shift differences upon binding NPF-containing peptides as its HSQC cross-peak disappeared upon peptide addition and did not reappear even at higher peptide:protein ratios presumably because of another exchange broadening mechanism. Phe^{40} is located at the end of helix B, and its amide hydrogen forms a hydrogen bond with the carbonyl of Ala^{36}.

The chemical shift changes of the EH domain upon addition of **NPF**$_{cyc}$ are mapped onto the tertiary structure of the EH domain (Figure 5A). NPF peptide binding predominantly affected residues in the second and third helices. Phe^{40}, Leu^{50}, Ser^{51}, and Trp^{54} are found at the base of a hydrophobic pocket formed from residues from these two helices. Other conserved, mostly hydrophobic residues, Thr^{41}, Ile^{47}, and Leu^{48}, line the pocket. The calcium binding residues dominate an electronegative patch adjacent to the NPF binding site (Figure 5B). Comparison of the electrostatic potential map and the convex−concave map (Figure 5C) shows that the hydrophobic binding pocket is bracketed on the left by a positive charge contributed by Lys^{37} and on the right by a negative charge from Glu^{55}. These residues partially occlude access to the binding site. The backbone amide groups of these residues showed significant chemical shift differences (>0.2 ppm in ^{1}H or 2 ppm in ^{15}N) upon peptide binding, suggesting that they change conformation and thus form a gate over the binding site.

Fast Exchange Binding Analysis. Analysis of progressive changes in chemical shifts as peptide was added indicated 1:1 binding (Figure 6A). Substantial line broadening at substoichiometric peptide:protein ratios (Figure 6B) suggested that the dissociation of the complex occurred with a

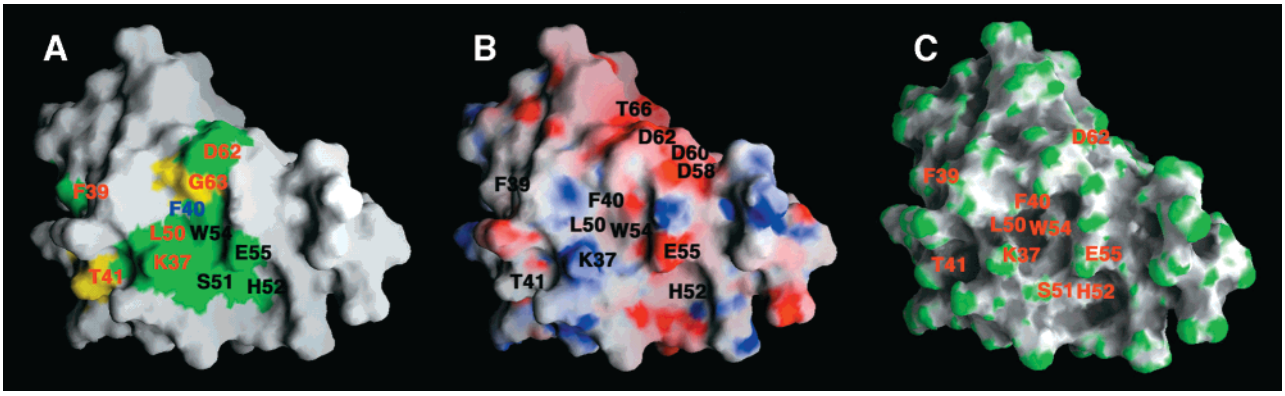

FIGURE 5: NPF-binding surface of the Reps1 EH domain. (A) A molecular surface model showing the NPF binding site. NMR chemical shift changes of the backbone amide group are represented by green surfaces for changes larger than 0.2 ppm and yellow surfaces for changes larger than 0.15 ppm. Residues that exhibit significant shifts are identified by residue number. Residue numbers for residues that do not shift upon addition of a DPF-containing peptide are shown in black. Residue 40 (blue) disappears on binding the NPF-containing peptides and broadens substantially with an NPY-containing peptide. (B) A model showing electrostatic potentials for surface residues. The potential is blue for basic residues and red for acidic residues. Residues that exhibit significant changes in chemical shift on adding NPF-containing peptides or that ligand the calcium ion are indicated by residue number. (C) A model showing the surface topology of the EH domain. Surfaces are depicted with green for convex surfaces and gray for concave. The largest hydrophobic binding pocket is centered on Trp[54]. Molecular surfaces were generated with GRASP (*39*).

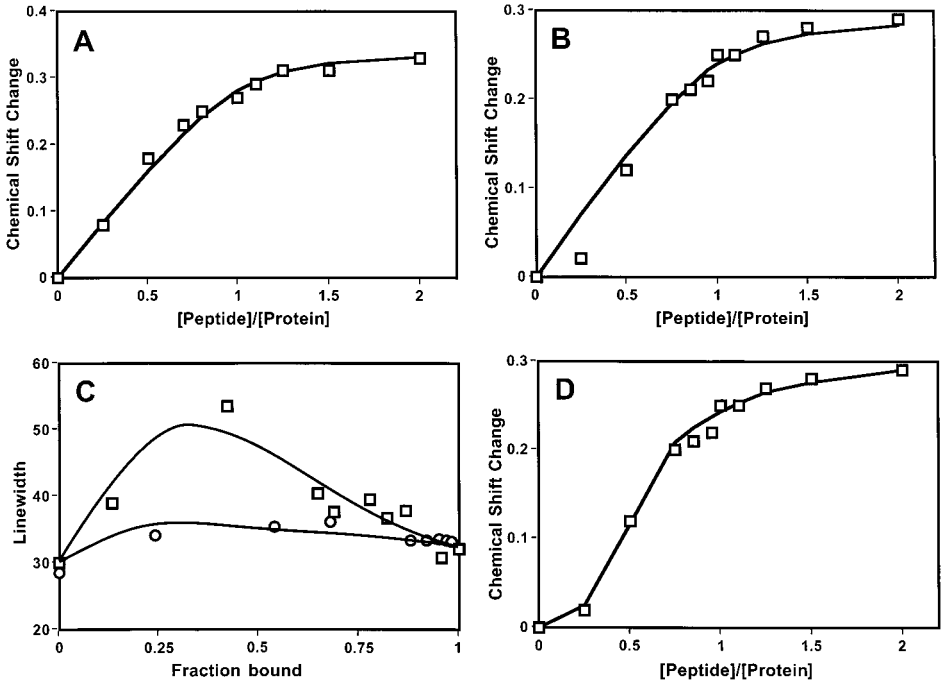

FIGURE 6: Binding analysis of the interaction of the EH domain with NPF-containing peptides. The chemical shift changes and line width perturbations caused by the binding of **NPF**$_{cyc}$ and **NPF**$_{lin}$ peptides were analyzed using an assumption of fast exchange (A−C) and using a simulation method, including effects of intermediate exchange (D). (A) Change in chemical shift for the ^{1}H resonance of the side chain of Trp[54] during titration by the **NPF**$_{lin}$ peptide. The line drawn through the points was calculated with an equilibrium dissociation constant (K_d) of 28 μM. (B) Change in the ^{1}H resonance of Trp[54] during titration by the **NPF**$_{cyc}$ peptide. The line drawn through the points was calculated with an equilibrium dissociation constant (K_d) of 27 μM. (C) Line width changes for Trp[54] [(□) **NPF**$_{cyc}$ peptide and (○) **NPF**$_{lin}$ peptide]. The calculated line was drawn using a dissociation rate constant (k_{off}) of 700 s^{-1} for the **NPF**$_{cyc}$ peptide titration and 1800 s^{-1} for the **NPF**$_{lin}$ peptide. (D) Titration with the **NPF**$_{cyc}$ peptide for the side chain of Trp[54] with the line drawn calculated with a K_d of 43 μM and a k_{off} of 430 s^{-1}.

lifetime approaching the frequency difference between the free and bound protein and therefore the presence of intermediate exchange. In practice, the assumption of fast exchange is usually made to facilitate the analysis for cases between fast and intermediate exchange since there is no simple test to establish whether the fast exchange condition is completely fulfilled (*16*). Therefore, equilibrium dissociation constants (K_d) were initially estimated from a simple plots of $\Delta\delta$ versus the ratio of peptide to protein concentration (Figure 6).

The linear peptides were relatively easy to analyze assuming only fast exchange. For **NPF**$_{lin}$, several resonances could be followed throughout the titration that gave an average K_d of 46 ± 14 μM (see the Supporting Information). The data extracted for the titration following the ^{1}H resonance of the side chain of Trp[54] in the bottom of the binding pocket show a fit with a K_d of 28 ± 17 μM (Figure 6A). For **DPF**, the average K_d was 530 ± 210 μM, and for **NPY**, the average K_d was 1080 ± 320 μM. For the cyclic peptide, however, experimental binding curves for all residues showed signifi-

cant sigmoid character, i.e., a systematic deviation from the hyperbolic curves calculated in the fast exchange limit. The fits for **NPF**$_{cyc}$ were poor with K_d values averaging 151 μM with a large standard deviation ($\pm$141 μM). For example, for the ^{1}H resonance of the side chain of Trp^{54}, the best fit was obtained with a K_d of 27 $\pm$ 32 μM (Figure 6B). It is interesting to note that the ^{1}H shift for Trp^{54} was larger for **NPF**$_{lin}$ (0.35 $\pm$ 0.02 ppm) than for **NPF**$_{cyc}$ (0.29 $\pm$ 0.03 ppm). The ^{15}N shift for this residue followed the usual pattern of being $\sim$60% larger for **NPF**$_{cyc}$ than for **NPF**$_{lin}$.

During the titration, line broadening due to chemical exchange was observed and its extent measured (Figure 6C). The Trp^{54} resonances of the EH domain were well-resolved throughout the titration with **NPF**$_{cyc}$ and **NPF**$_{lin}$ and showed a large and small effect, respectively. At substoichiometric peptide:protein ratios, broader lines were observed for almost all residues of the cyclic peptide than for those of the linear peptide. Dissociation rate constants (k_{off}) were estimated using eq 8. Although the experimental points have significant scatter, the best fits gave a k_{off} of 700 $\pm$ 250 s^{-1} for the cyclic peptide and 1800 $\pm$ 250 s^{-1} for the linear peptide.

Intermediate Exchange Binding Analysis. Substantial errors can be made in K_d or the estimated value for the chemical shift of the complex if using fast exchange analysis under conditions where $k_{off} \leq 1000$ s^{-1} (*16*, *29*). Although there is no analytical equation for calculating the peak position (i.e., the binding curve) for intermediate exchange, the full line shape (amplitude vs relative chemical shift difference) can be calculated. Although the first and second derivatives of the curve may be determined numerically (*16*), we found it more practical to examine the calculated curve following minor adaptations of previously published protocols (*28*, *29*). The calculated line shape is dependent on the K_d, k_{off}, the line width, and the chemical shift difference between free and bound states. We simulated peak shapes for each titration point for several residues that could be followed throughout the titration. Figure 6D shows the best-fit binding curve for the ^{1}H resonance of the side chain of Trp^{54}. Inclusion of the k_{off} term dropped χ^2 from 0.035 in Figure 6B to 0.007 in Figure 6D. The K_d was determined to be 43 μM and k_{off} to be 440 s^{-1}. The average over several residues yielded a K_d for **NPF**$_{cyc}$ of 65 $\pm$ 17 μM and a k_{off} of 440 $\pm$ 110 s^{-1}. These numbers were more accurate than the analysis used without consideration of intermediate exchange (cf. Figure 6A and the top curve of Figure 6C).

For **NPF**$_{lin}$, inclusion of an intermediate exchange term with a k_{off} of 1800 s^{-1} calculated from the line width analysis (Figure 6C) improved the fit to the experimental data in Figure 6A (but not significantly, dropping the χ^2 only slightly from 0.007 to 0.006). Because the chemical shifts are influenced little by intermediate exchange for **NPF**$_{lin}$, a more accurate value was obtained from line width analysis.

The binding curves show that most residues have small additional shifts at high peptide:protein ratios (e.g., Figure 6D). These may reflect nonspecific binding of the peptide to the protein, although it is difficult to rationalize why these would cause the same chemical shift changes as the specific binding. Alternatively, a small error in protein or peptide concentration ($\sim$10%) could also account for most of the discrepancy between the fit and the data.

Although the preliminary analysis for k_{off} indicated that intermediate exchange must be considered, more complicated binding stoichiometries could influence the binding curve. For example, the complex may show two states that are in conformational exchange (*35*). Alternatively, the peptide could first fill a limited number of tight binding sites on the glass wall of the NMR tube. However, we have shown that the off rates are such that intermediate exchange is altering the change in chemical shift such that the change no longer is linearly related to the fraction bound (f_b). With consideration of intermediate exchange, the data can be fit to within experimental error.

DISCUSSION

Structure of the Reps1 EH Domain. The Reps1 EH domain comprises two helix−loop−helix motifs characteristic of EF-hand domains (*36*). This structure has been also identified in the EH domains of mouse and human Eps15 (*11*, *12*, *37*) and that of POB1 (*10*). The overall fold of the Reps1 EH domain is shared with these EH domains, except that the mouse EH$_1$ domain contains additional short helices at its N- and C-termini. Comparison of the known EH domain structures with the amino acid sequences shows that the structurally critical residues involved in the packing of the hydrophobic core are highly conserved throughout the family. Interestingly, five of seven highly conserved hydrophobic residues are phenylalanines (Phe^{20}, Phe^{39}, Phe^{40}, Phe^{70}, and Phe^{74}) which form a structural core. The interaction of these conserved structural residues allows the different EH domains to adopt similar folds.

Superposition of the helical residues of the Reps1 EH domain on the Eps15 EH$_1$−EH$_3$ domains resulted in rms deviations for the backbone atoms of 2.4 $\pm$ 0.1, 2.1 $\pm$ 0.1, and 2.1 $\pm$ 0.2 Å, respectively. However, if the helix A was not included in the comparison, the rms deviations for the Reps1 EH domain became 1.2 $\pm$ 0.1, 1.4 $\pm$ 0.1, and 1.0 $\pm$ 0.3 Å, respectively (see the Supporting Information). A similar change was observed in the comparison of the four major helices of the EH$_1$ domain with the EH$_2$ and EH$_3$ domains ($\sim$2.3 Å), which dropped to $\sim$1.3 Å when the first helix was ignored. Calculation using INTERHLX (*38*) showed the angles between the helices of Reps1 are mostly unchanged relative to the EH$_2$ and EH$_3$ domains, but that the deviation results from a $\sim$2 Å displacement of helix A from the bundle of the helices B−D. In summary, the four helices of the EH domains superimpose only moderately well and helix A shows a variable position with respect to the other three helices. Comparisons of the four EH domain structures also show large variations in the conformations of the calcium-free loop (residues 25−32) between helices A and B (see the Supporting Information) and of the C-terminal proline-rich region.

Specificity of NPF Peptide Binding. The residues that exhibit large changes in chemical shifts are observed to form part of a hydrophobic pocket between helices B and C (Figure 5). This observation is consistent with the recently determined structure of the Eps15 EH$_2$ domain in complex with an NPF-containing peptide (*34*). Mutational analysis of the Eps15 EH$_2$ domain showed that the hydrophobic character of Trp^{169} and Leu^{165} (corresponding to Trp^{54} and Leu^{50} of Reps1) is critical for binding (*27*). The position of the Trp^{54} side chain in Reps1 was precisely defined by more than 30 NOEs between the Trp^{54} aromatic ring and residues

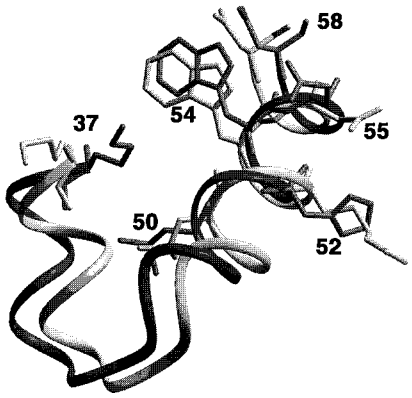

FIGURE 7: Superposition of the NPF peptide binding site of the Reps1 EH domain (dark gray) with the second EH domain from Eps15 (light gray). Residues within the core of the binding pockets that contribute to NPF binding and specificity are indicated.

in the calcium binding loop. NMR studies of the human EH_2 domain and the calcium-free EH_1 domain from mouse Eps15 show a similar hydrophobic pocket as the primary interaction site. Comparison of the EH sequences indicates that the hydrophobic residues in the binding site are conserved. Therefore, the interaction between hydrophobic residues of the binding pocket and the NPF core sequence seems to be a general mechanism of binding.

Binding to a specific target protein is the biological function of an individual EH domain. Some EH domains prefer to bind to peptides with FW, WW, or SWG motifs, whereas the other EH domains bind only peptides bearing NPF (*27*). The NPF sequence motif appears to be critical for binding to the Reps1 EH domain because of its ability to select NPF-containing proteins in a yeast two-hybrid experiment and because the affinity for DPF- or NPY-containing peptides is substantially decreased ($K_d = 0.5-1$ mM) compared to the corresponding linear NPF peptide ($K_d = 46 \pm 14$ μM).

Among the EH domains that target NPF-containing peptides, different binding specificity may influence which NPF-containing target protein is bound. The Reps1−$\mathbf{NPF}_{lin}$ complex ($K_d = 46 \pm 14$ μM) appears to be much tighter than the corresponding complex formed by the Eps15 EH_2 domain ($K_d = 560 \pm 40$ μM), although this difference may be attributable to the different amino acid sequences flanking the core NPF (*12*). Cyclization of the target peptide by incorporation of a disulfide bond has a much larger effect on the Eps15 complex ($K_d = 12 \pm 2$ μM) than observed here on the Reps1 complex ($K_d = 65 \pm 17$ μM) (*34*). In an ELISA-style pull-down experiment (*18*), the Reps1 EH domain did not bind to $\mathbf{NPF_{RAB}}$, although the Eps15 EH_2 domain does (M. Yamabhai and B. Kay, personal communication).

The structure of the Reps1 EH domain suggested a gate formed by residues Lys^{37} and Glu^{55} over the hydrophobic NPF-binding pocket (Figure 5). A change in the conformation of these gate residues may explain the difference in specificity between the Reps1 EH and Eps15 EH_2 domains. The binding sites of the Reps1 EH and Eps15 EH_2 domains are compared in Figure 7. The overall conformation of the pocket formed by helices B and C and the orientation of the side chains of conserved hydrophobic residues are roughly equivalent, but the two charged side chains (Lys^{37} and Glu^{55}) are positioned differently. The distance from Lys^{37} ζ_N to the closest Glu^{55} ϵ oxygen is 8.5 ± 1 Å in the Reps1 EH domain, whereas it is 13 ± 1 Å in the Eps15 EH_2 domain (either alone or in complex with a peptide). The difference is not caused by undefined side chain structure in the Reps1 EH domain since nine NOE restraints were observed for the Lys^{37} side chain and seven for the Glu^{55} side chain and χ_1 angle restraints for both were used in the structure calculation or in the Eps15 EH_2 domain since the same conformations for the gate residues are observed both in the free protein and in complex with NPF-containing peptides. The difference may arise in part from the change in neighboring residue 52. Arg^{52} in Eps15 appears to interact more favorably with Glu^{55} than the short chain, partially charged His^{52} residue in the Reps1 EH domain. Residues Glu^{55} and Lys^{37} have also been suggested to be important for specific recognition by the Eps15 EH_3 domain. Site-directed mutations of Arg^{249} of the Eps15 EH_3 domain (corresponding to Lys^{37} in Reps1) to lysine and alanine each showed a much more dramatic decrease in NPF peptide affinity than with the corresponding EH_2 (K152A) mutant, suggesting that the gate residues have different roles in different EH domains (*37*).

Binding Analysis. The methods we used to analyze the NMR titration data can be applied to the complete range of exchange regimes to obtain accurate binding parameters. Most texts describe the influence of exchange in a system with equal fractions of the two populations. In systems where ratios vary (which occurs during the course of a titration), the calculations showed that the influence of intermediate exchange on the peak position is dependent on the peptide:protein ratio. To take a dramatic theoretical example using a k_{off} of 200 s^{-1}, a $\Delta\delta$ of 100 Hz, and a K_d of 1 μM, at a 0.1 peptide:protein ratio two peaks would appear in slow exchange. At a 1:1 ratio, the peak would be in intermediate exchange, and at a 10:1 ratio, one peak would show in fast exchange between free and bound states.

For $\mathbf{NPF}_{lin}$, from the observed K_d ($=k_{on}/k_{off}$) of 46 ± 14 μM and k_{off} of 1800 ± 250 s^{-1}, the calculated k_{on} is $0.3-0.6 \times 10^8$ M^{-1} s^{-1}, which is near the diffusion-controlled limit ($\sim 1 \times 10^8$ M^{-1} s^{-1}). For the cyclic peptide, an association rate constant (k_{on}) was estimated to be 7×10^6 M^{-1} s^{-1}, which is 10−50-fold slower than diffusion. The ~60% larger chemical shift changes observed upon binding the cyclic peptide and the off rates indicate that the Reps1 EH domain must undergo greater conformational changes to bind $\mathbf{NPF}_{cyc}$ than to bind $\mathbf{NPF}_{lin}$. The cyclic peptide exhibited a slightly weaker binding affinity than its linear counterpart for the Reps1 EH domain in contrast to results with the Intersectin EH domain (*18*).

The recently published structure of the EH_2 domain in complex with a linear NPF-containing peptide (*34*) allows an interpretation of some of the chemical shift changes that were observed for Reps1. The largest chemical shift changes occurred in the binding site identified by intermolecular NOEs between the EH_2 domain and NPF. However, some smaller changes cannot be so readily interpreted. For example, the binding of **NPY**, although weaker, shows mostly the same changes in chemical shift as the NPF-containing peptides, and, when extrapolated to saturation, the same extent of change. The EH_2−peptide complex shows room for a hydroxyl instead of the hydrogen on Cζ of the phenylalanine ring (*34*). If the Reps1 EH domain complex

with **NPY** is assumed to be isosteric with the EH_2 domain complex, the hydroxyl of **NPY** is then placed in a hydrophobic environment comprising the side chains of Ala^{36}, Phe^{40}, and Trp^{54} without possible hydrogen bond acceptors and donors. This may account for the much lower affinity of **NPY** in comparison with that of $\mathbf{NPF}_{lin}$.

The Reps1 EH domain showed quite different chemical shifts when binding **DPF** than when binding NPF-containing peptides. As illustrated in Figure 5A, the binding of **DPF** no longer caused chemical shift changes for residue 51, 52, 54, or 58, despite these residues showing the largest changes on binding NPF. This is consistent with the EH_2−NPF complex structure which suggests hydrogen bond acceptance of the asparagine side chain by the carbonyl of residue 51 or 52. In addition, intermolecular NOE cross-peaks were observed between the γ-NH_2 group of the asparagine and the amide hydrogens of residues of the EH_2 domain that correspond to residues 54−56 of Reps1 (*34*). Therefore, we conclude that the Reps1 EH domain also uses residues 51−58 for recognition of the asparagine of the NPF motif.

The binding of peptides affects resonances for some residues located away from the primary interaction site. For example, chemical shift changes were observed on the side chain NH_2 group of Gln^{19}, which is >20 Å away from the NPF-binding site on the far side of the conserved phenylalanine cluster that makes up a large part of the hydrophobic core of EH domains. Phe^{40} is clearly part of the NPF-binding site (*34*) and also part of the phenylalanine cluster. We speculate that small conformational changes result in a global effect transmitted through the hydrophobic core from Phe^{40} on one side of the core to Gln^{19} on the other side. In binding $\mathbf{NPF}_{lin}$, the change was ~0.05 ppm for ^1H and the change was ~0.5 ppm for ^{15}N (Figure 3). However, we cannot explain why on binding **DPF** the chemical shift changes were in the same direction as when binding NPF, but were about 3 times larger (0.2 ppm for ^1H and 1.5 ppm for ^{15}N).

It was predicted from the structure of the EH_2−NPF complex that a peptide containing DPF should not bind because of electrostatic repulsion from the side chain of Glu^{170} (Glu^{55} in Reps1). However, perhaps because of the different arrangement for the gate residues (Glu^{55} and Lys^{37}) noted above, the Reps1 domain was observed to have weak but significant binding to a DPF sequence with a K_d of 0.5 ± 0.2 mM that is about the same strength as that reported for the Eps15 EH_2 domain binding to $\mathbf{NPF}_{RAB}$ (*12*). Eps15 contains three EH domains in its N-terminus and 15 DPF motifs in its C-terminus. The ability of full-length Eps15 to form a tetramer has been attributed to EH domain−DPF interactions (*5*). In addition, the POB1 EH domain, a close homologue of the Reps1 EH domain, has been observed to bind directly to a region in the C-terminus of Eps15 that does not contain NPF, but contains 12 DPF motifs. The possibility that EH domains recognize DPF as well as NPF therefore cannot be dismissed.

ACKNOWLEDGMENT

We thank Dr. Jim Sudmeier for assistance with binding analysis and with setting up the NMR experiments at Tufts University and Dr. Susan Pochapsky for help at the Francis Bitter Magnet Lab at the Massachusetts Institute of Technology (Cambridge, MA). We also thank Tricia McCampbell in the study involving DPF- and NPY-containing peptides, Montarop Yamabhai and Brian Kay for sharing results prior to publication, and Gillian Henry for a critical review of the manuscript.

SUPPORTING INFORMATION AVAILABLE

Tables of titration data and structural analysis. This material is available free of charge via the Internet at http://pubs.acs.org.

REFERENCES

1. Fazioli, F., Minichiello, L., Matoskova, B., Wong, W. T., and Di Fiore, P. P. (1993) *Mol. Cell. Biol. 13*, 5814−5828.
2. Marsh, M., and McMahon, H. T. (1999) *Science 285*, 215−220.
3. Ikura, M. (1996) *Trends Biochem. Sci. 21*, 14−17.
4. Nakashima, S., Morinaka, K., Koyama, S., Ikeda, M., Kishida, M., Okawa, K., Iwamatsu, A., Kishida, S., and Kikuchi, A. (1999) *EMBO J. 18*, 3629−3642.
5. Cupers, P., ter Haar, E., Boll, W., and Kirchhausen, T. (1997) *J. Biol. Chem. 272*, 33430−33434.
6. Yamaguchi, A., Urano, T., Goi, T., and Feig, L. A. (1997) *J. Biol. Chem. 272*, 31230−31234.
7. Bos, J. L. (1998) *EMBO J. 17*, 6776−6782.
8. Ikeda, M., Ishida, O., Hinoi, T., Kishida, S., and Kikuchi, A. (1998) *J. Biol. Chem. 273*, 814−821.
9. Kariya, K., Koyama, S., Nakashima, S., Oshiro, T., Morinaka, K., and Kikuchi, A. (2000) *J. Biol. Chem. 275*, 18399−18406.
10. Koshiba, S., Kigawa, T., Iwahara, J., Kikuchi, A., and Yokoyama, S. (1999) *FEBS Lett. 442*, 138−142.
11. Whitehead, B., Tessari, M., Carotenuto, A., van Bergen en Henegouwen, P. M., and Vuister, G. W. (1999) *Biochemistry 38*, 11271−11277.
12. de Beer, T., Carter, R. E., Lobel-Rice, K. E., Sorkin, A., and Overduin, M. (1998) *Science 281*, 1357−1360.
13. Enmon, J. L., de Beer, T., and Overduin, M. (2000) *Biochemistry 39*, 4309−4319.
14. Matsuo, H., Walters, K. J., Teruya, K., Tanaka, T., Gassner, G. T., Lippard, S. J., Kyogoku, Y., and Wagner, G. (1999) *J. Am. Chem. Soc. 121*, 9903−9904.
15. Rajagopal, P., Waygood, E. B., Reizer, J., Saier, M. H., Jr., and Klevit, R. E. (1997) *Protein Sci. 6*, 2624−2627.
16. Feeney, J., Batchelor, J. G., Albrand, J. P., and Roberts, G. C. K. (1979) *J. Magn. Reson. 33*, 519−529.
17. Fersht, A. (1985) *Enzyme structure and mechanism*, 2nd ed., Freeman, New York.
18. Yamabhai, M., Hoffman, N. G., Hardison, N. L., McPherson, P. S., Castagnoli, L., Cesareni, G., and Kay, B. K. (1998) *J. Biol. Chem. 273*, 31401−31407.
19. Yamaguchi, A., Urano, T., Goi, T., and Feig, L. A. (1997) *J. Biol. Chem. 272*, 31230−31234.
20. Kim, S., Dubelman, A. M., Goonesekera, S., Feig, L. A., and Baleja, J. D. (2000) *J. Biomol. NMR 18*, 367−368.
21. Pace, C. N., Vajdos, F., Fee, L., Grimsley, G., and Gray, T. (1995) *Protein Sci. 4*, 2411−2423.
22. Wagner, G., Braun, W., Havel, T. F., Schaumann, T., Go, N., and Wüthrich, K. (1987) *J. Mol. Biol. 196*, 611−639.
23. Brünger, A. T. (1987) *X-PLOR: A system for X-ray crystallography and NMR*, Yale University Press, New Haven, CT.
24. Linge, J. P., and Nilges, M. (1999) *J. Biomol. NMR 13*, 51−59.
25. Strynadka, N. C., Cherney, M., Sielecki, A. R., Li, M. X., Smillie, L. B., and James, M. N. (1997) *J. Mol. Biol. 273*, 238−255.
26. Chattopadhyaya, R., Meador, W. E., Means, A. R., and Quiocho, F. A. (1992) *J. Mol. Biol. 228*, 1177−1192.
27. Paoluzi, S., Castagnoli, L., Lauro, I., Salcini, A. E., Coda, L., Fre, S., Confalonieri, S., Pelicci, P. G., Di Fiore, P. P., and Cesareni, G. (1998) *EMBO J. 17*, 6541−6550.
28. Nakagawa, T. (1966) *Bull. Chem. Soc. Jpn. 39*, 1006−1008.

29. Sudmeier, J. L., Evelhoch, J. L., and Jonsson, N. B.-H. (1980) *J. Magn. Reson. 40*, 377−380.
30. Clore, G. M., and Gronenborn, A. M. (1994) *Methods Enzymol. 239*, 349−363.
31. Laskowski, R. A., Macarthur, M. W., Moss, D. S., and Thornton, J. M. (1993) *J. Appl. Crystallogr. 26*, 283−291.
32. Kay, L. E., Forman-Kay, J. D., McCubbin, W. D., and Kay, C. D. (1991) *Biochemistry 30*, 4324−4333.
33. Cates, M. S., Berry, M. B., Ho, E. L., Li, Q., Potter, J. D., and Phillips, G. N., Jr. (1999) *Struct. Folding Des. 7*, 1269−1278.
34. de Beer, T., Hoofnagle, A. N., Enmon, J. L., Bowers, R. C., Yamabhai, M., Kay, B. K., and Overduin, M. (2000) *Nat. Struct. Biol. 7*, 1018−1022.
35. Baldo, J. H., Halford, S. E., Patt, S. L., and Sykes, B. D. (1975) *Biochemistry 14*, 1893−1899.
36. Strynadka, N. C., and James, M. N. (1989) *Annu. Rev. Biochem. 58*, 951−998.
37. Enmon, J. L., de Beer, T., and Overduin, M. (2000) *Biochemistry 39*, 4309−4319.
38. Tjandra, N., and Yap, K. (2000) INTERHLX (http://nmr.uhnres.utoronto.ca/ikura/datasoft.html).
39. Nicholls, A., Sharp, K. A., and Honig, B. (1991) *Proteins 11*, 281−296.

BI002700M